

Effect of Inter-Electrode Distances of Glow Discharge On Structural and Optical Properties of ZnSe

E. R. Shaaban^{1,*}, F. Diab², G. M. El-Kashef², K. M. Ahmed², M. E. Abdel-kader² and W. H. Gaber²

¹Physics Department, Faculty of Science, Al-Azhar University, P.O. 71452, Assiut, Egypt.

²Plasma and Nuclear Fusion Department, N. R. C. Atomic Energy Authority, Egypt.

Received: 2 Jan. 2016, Revised: 22 Jan. 2016, Accepted: 24 Jan. 2016.

Published online: 1 Jul. 2016.

Abstract: A glow discharge device is constructed and operated by using Ar gas. Paschen curve is analyzed at different pressures and inter-electrode distances. The experimental results show that the discharge is optimized at 5cm inter-electrode distance. The I-V characteristic of the glow discharge at different pressures is studied and the Zinc selenide (ZnSe) thin film is treated. The effect of exposure to the Ar plasma immersion-ion-implantation at different inter-electrode spacing (5, 8.5, 11.5 and 14.5 cm) on the microstructure parameters and energy gap of ZnSe thin film are investigated. It is observed that, both crystallize size and lattice strains are increased by increasing the inter-electrode distances. The values of absorbance in strong absorption region are reduced with increasing the inter-electrode spacing. In addition, the optical band gap E_g^{opt} has been determined in terms of absorbance curves and found to be increased with the Paschen's minimum, when inter-electrode spacing increases.

Keywords: Glow Discharge, Paschen Curve, Inter-electrode, ZnSe, Thin Film.

1 Introduction

The simplified configuration of parallel plates-electrodes is used to find the breakdown voltage of the surface glow discharge [1]. The electrical voltage should have high value enough in order to ignite the breakdown of the gas. The characteristics of the plasma are controlled by four variables: potential difference, distance between the electrodes, pressure and a type of gas, and electrode material. The breakdown voltage is a function of the product pd (gas pressure, distance between the electrodes) [2, 3]. The glow discharge investigated for variable inter-electrode gaps and radii of the discharge tubes [4]. The curve of breakdown voltage (V_B) has high value at low and high gas pressure, because the mean free path is large in low pressure so the particles need high energy to ionize and accelerate while at high gas pressure the mean free path is small so the energy loss is large [5]. Theoretically, the dependence of V_B on p and d is not always that simple [6] and experimentally, Paschen law is valid only for discharge tubes which the dimensions of the electrodes and the distances between them are geometrically similar [4]. The linear form of the I-V curve indicates that the potential between the two electrodes increases with the current [7].

The DC gas discharge is used for different applications such as: surface modification, lamps, plasma displays, lasers, biomedical applications, particle sources [8, 9], thin films deposition, etching, plasma polymerization, and pumping gas discharge lasers [10, 11]. Thin films are material layers with thickness ranging from a few atomic layers (\sim nm) to a few micrometers [1, 12]. There are various ways to produce thin films; chemical vapor deposition, laser evaporation, heat evaporation, plasma assisted evaporation [4, 13]. The thin film in glow discharge ion source is formed by the sputtering process. The sputtering process is the ejection of atoms by the bombardment of a target by the ions [14]. The number of sputter ejected atoms and the number of incident projectiles is the sputter yield; Y [15]. The ions and electrons are accelerated towards the cathode and the anode by this electric field respectively. Substrates with film deposition may be etched, cleaned and modified by various sputtering techniques [16]. The sample treated with plasma at a current of 50mA, pressure 0.2 torr, voltage 235 v and power of 11.75 W.

Zinc selenide (ZnSe) is an attractive semiconductor material for optoelectronic device applications [17]. Development of small integrated circuits, suitable for future generation Giga Scale Integration (GSI) technology, requires advanced

*Corresponding author e-mail: esam_ramadan2008@yahoo.com

materials and new processing techniques [18]. The technology of thin films which was primarily developed for the integrated circuit industry, is able to play an important role in achieving this goal. Therefore, now days thin films technology is being adopted by the high-tech industries [19]. Some of the important applications of thin films have been studied in communication, microelectronics, catalysis, optical electronics, energy generation and conservation strategies. Plasma Immersion Ion Implantation (PIII) process is a three dimensional surface modification method that is quite mature and well known to the surface engineering community nowadays, specially to those working in the field of plasma-materials interaction, aiming at both industrial and academic applications. Plasma Immersion Ion Implantation and deposition (PIII&D) is becoming a routine method of surface modification, with the advantage of pushing up the retained dose levels limited by the sputtering owing to ion implantation. Therefore, well adherent, thick, three-dimensional films without stress are possible to be achieved, at relatively low cost, using PIII&D. The gas plasma treatments have been probed as a suitable technology for the modification on the optical characteristic of the films [20-22]. The present work was examined the changes in microstructure parameters and the energy gap of ZnSe thin films due to plasma-immersion with Ar gas at different inter-electrode distances 5, 8.5, 11.5 and 14.5 cm. Interpretation of the change in energy gap in terms the change in microstructure parameters.

2 Experimental Details

The experimental setup of glow discharge device is shown in Fig. 1. The vacuum chamber is a cylindrical shape made of a Pyrex glass with 30 cm length, 18 cm diameter and 8 mm thickness, closed by Aluminum plates and sealed by O-rings. The two electrodes are made of Aluminum with diameter of 15 cm where the anode is a movable electrode. The discharge chamber is evacuated to a base pressure down to 10^{-2} torr by a vacuum system (Alcatel Rotary). The working gas is high purity argon gas and fed to the discharge chamber through a needle valve. The pressure of the gas is varied from 0.2 to 1 torr. The applied voltage between the two electrodes (see Fig. 1) is controlled by a DC power supply which can produce potential up to 4 kV and 60 mA. A DC glow discharge is initiated between the two electrodes at a pressure of 0.2 torr. The voltage and current are measured by voltmeter and ammeter respectively. The breakdown voltage is analyzed at different values of pressure (0.2 to 1 torr) and inter-electrode distance (5, 8.5, 11.5 and 14.5 cm) to obtain the Paschen curve. I-V characteristic is detected at different argon pressures.

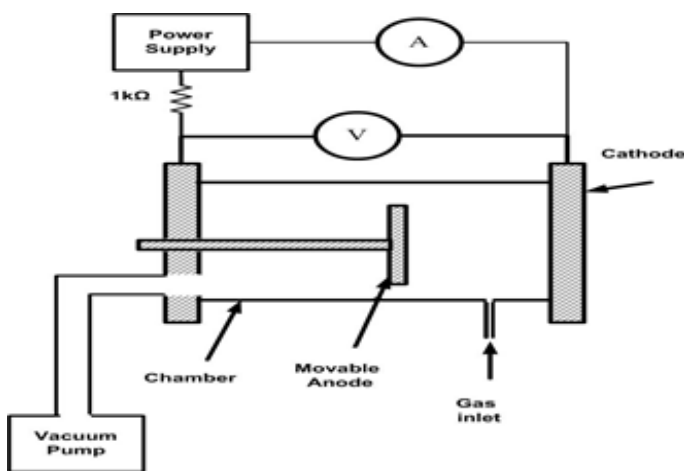


Fig. 1: A schematic diagram for the experimental equipment.

High purity ZnSe powder (99.999 %) from Aldrich Company was used. Thin films with different thicknesses were deposited by evaporating ZnSe powder onto ultrasonically cleaned glass substrate, which was kept at constant temperature of 373 K. The evaporation was carried out using thermal evaporation unit (Denton Vacuum DV 502 A) under vacuum of 10^{-6} Pa. The optimum conditions for the uniform films were obtained by mechanical rotation of the substrate holder at ~30 rpm during the deposition. Both the deposition rate (2 nm/s) and the film thickness were controlled using quartz crystal monitor DTM 100.

XRD analysis was done to study the crystal structure of prepared powder and thin films, where the diffractometer (Philips X-ray diffractometer, 1710) with Ni-filtered CuK_α radiation ($\lambda = 0.15418$ nm). The diffractometer was operated at a scanning step of $\Delta 2\theta = 0.02^\circ$, for a period of 5 s at every fixed value, to yield the reasonable number of counts for each peak. The absorbance measurements were carried out using a double-beam (Jasco V670) spectrophotometer, at normal incidence of light and in a wavelength range between 400 and 1100 nm.

3 Results and Discussions

The curve of breakdown voltage V_B is shown in Fig. 2 as a function of the product of the gas pressure p and the inter-electrode distance d . The breakdown voltage is measured for Ar gas in the range between pd equals 1.1 and 14.5 torr.cm (i.e. $p=0.2$ to 1.0 torr). Townsend [23] led to the understanding that the breakdown is an avalanche effect caused principally by the ionization of gas molecules by electrons accelerated by the electric field. If the electron gains sufficient energy between collisions to ionize gas atoms or gas molecules, then each collision gives rise to two electrons and an ion, allowing an avalanche effect eventually resulting in a spark. This avalanche can only occur when there are sufficient gas molecules between the electrodes, i.e. if the mean free path between collisions is much smaller than the distance between electrodes. If the pressure is too low, or if the gap is too small, the avalanche breakdown (Townsend theory) cannot take place. This absence of atoms or molecules is what gives the minimum in the Paschen curve. At large gaps or pressures, a linear relation breakdown voltage and electrode gap is found, while at very small gaps one has a “vacuum isolation”, where there are not enough gas atoms or molecules for the avalanche to occur.

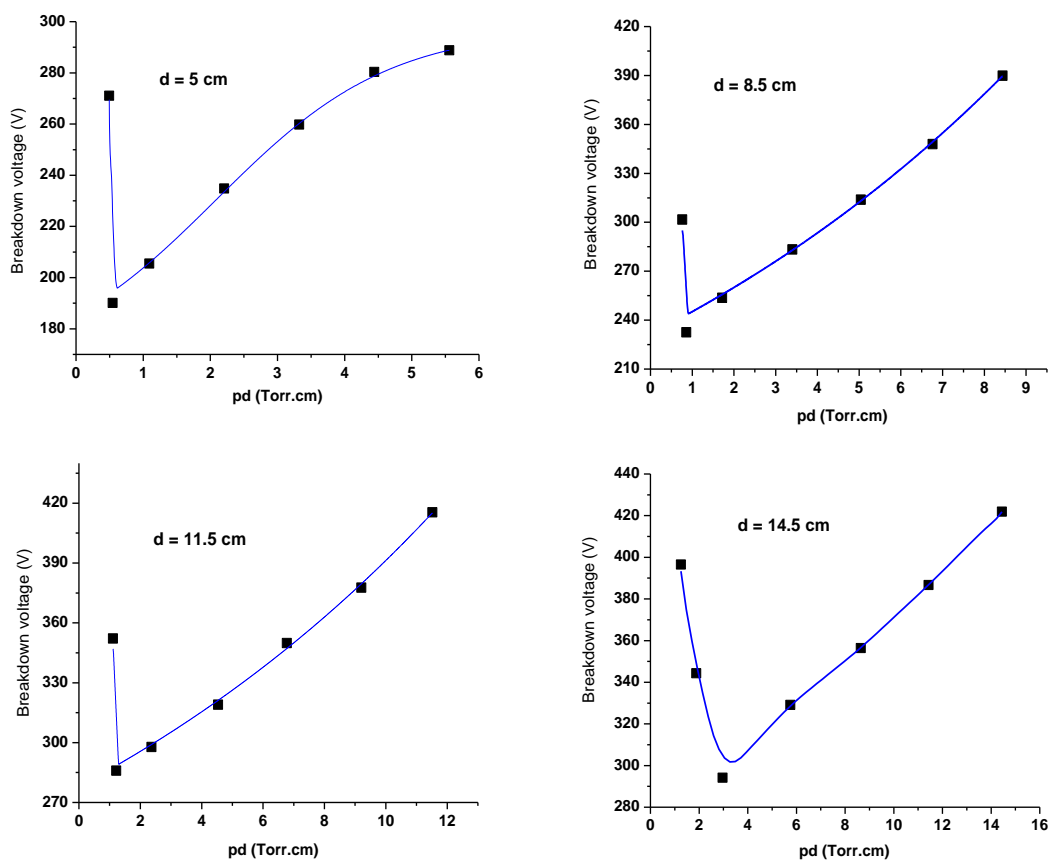


Fig. 2: A plot of breakdown voltage of Ar as a function of pd with different inter-electrode spacing.

According to the above Townsend theory, Fig. 2 shows Paschen's curves of Ar at different inter-electrode distances. A general remark of these curves is that, all the curves have nearly the same general behavior and obey the standard Paschen's curve. The breakdown voltage V_B initially decreases with increase in Pd , and then begins to increase with Pd after going through a minimum value. On the left-hand side of the minimum Paschen's curves, V_B decreases fast when increasing Pd which can be attributed to the increase in collision frequency, equivalent to an increase in the number of collisions between electrons and neutral atoms or molecules. However, on the right-hand side of the minimum, V_B increases slowly with the increase of Pd , i.e. the ionization cross-section increases. Therefore, electrons need more energy to breakdown the discharge gap, resulting in an increase of V_B . Fig. 3 shows a minimum value of breakdown voltage as a function of inter-electrode distance. The characteristics of glow discharge cathode current as a function of applied voltage for different argon gas pressure and at inter-electrode spacing equals to 5 cm have been established with the scheme shown in figure 4. The current in the external circuit can be measured as a function of voltage drop between the anode and the cathode.

Fig. 5 illustrates the XRD pattern of ZnSe thin films with inter-electrode distance The observed peaks of ZnSe thin films

were compared with the standard JCPDS values, which showed that the films also gives a structure matching with (JCPDS: 05-0566-cubic) zinc-blend cubic structure, with peaks at $2\theta = 28.56^\circ$, 47.52° and 56.29° corresponding to (111), (220) and (311) orientations, respectively.

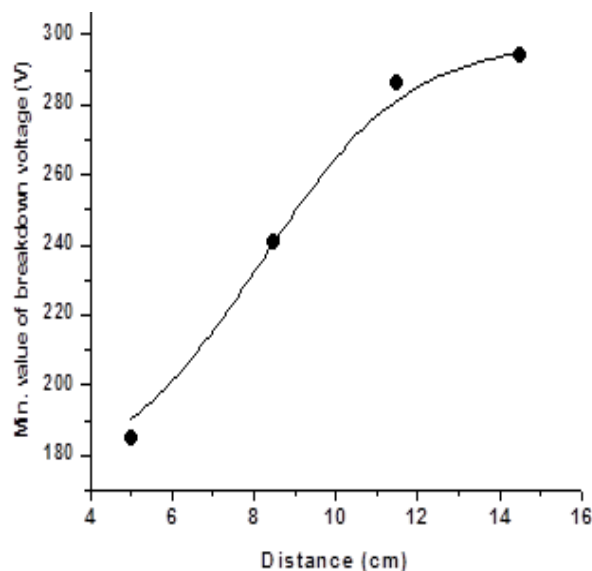


Fig. 3: Minimum values of breakdown voltage as a function of inter-electrode distance

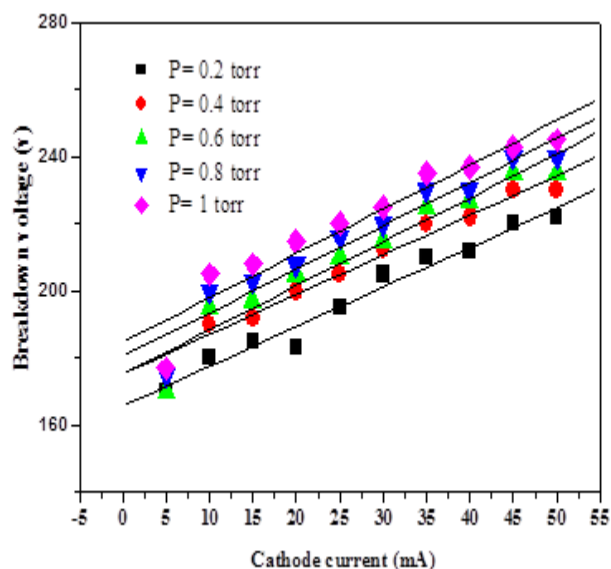


Fig. 4 I-V characteristics of Ar discharge plasma at different value of gas pressure and at inter-electrode spacing is 5 cm

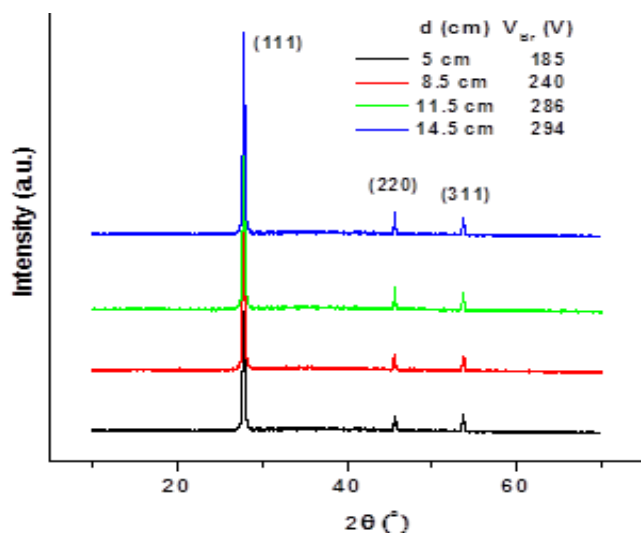


Fig. 5: XRD pattern of exposed ZnSe thin film at minimum value Paschen's curves of Ar, at different inter-electrode distances.

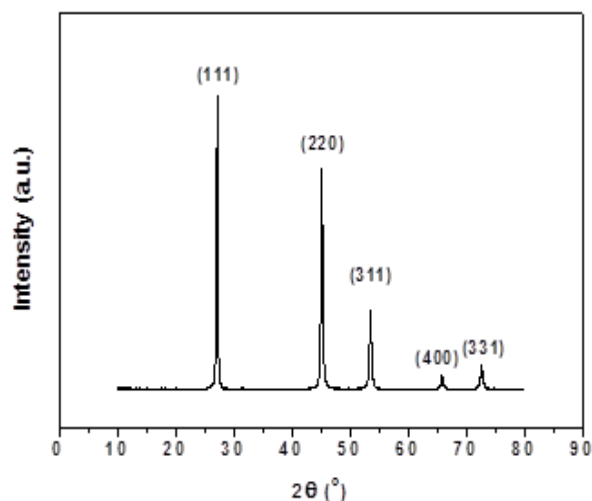


Fig. 6: X-ray diffraction spectra of ZnSe powder

Fig. 5 shows that the intensities of the peaks increase and the full width at half maximum (FWHM) decreases with increasing the inter-electrode distance. According to Williamson-Hall method [24-27], which discussed in details by Shaaban [28]. Fig. 6 displays the XRD diffractogram of ZnSe powder, which showed intense diffraction at $2\theta = 27.22$, 45.23 , 53.64 , 65.91 and 74.88 oriented along (111), (220), (311), (400) and (331) planes of polycrystalline ZnSe cubic phase (JCPDS: 05-0566). Fig. 8 and Fig. 9 illustrates crystallite size/strain separation calculating using $\beta 2\theta \cos(\theta_0)$ versus $\sin(\theta_0)$ according to "Williamson Hall" method. Both crystallite size and lattice strain increase with increasing the inter-electrode distance due to the reduction of FWHM. The increasing in crystallite size may attribute to the decreasing in the FWHM at each reflection when the increasing of the inter-electrode distance and also may be interpreted in terms of a columnar grain growth. Furthermore the microstrain displays the same behavior i.e. increasing with increasing the inter-

electrode distance. The microstrain behavior may be due to the decrease in lattice defects among the grain boundary.

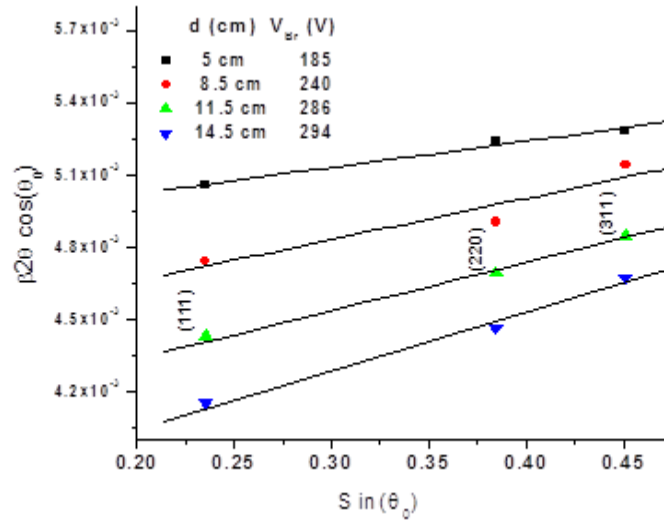


Fig. 7: Crystallite size/strain separation calculating using $\beta 2\theta \cos(\theta_0)$ versus $\sin(\theta_0)$ according to “Williamson Hall” method

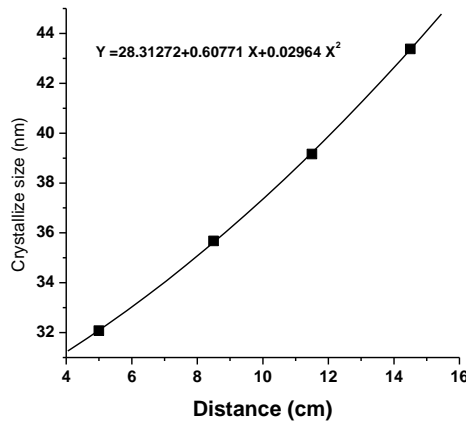


Fig. 8: Crystallite size as a function of inter-electrode distance

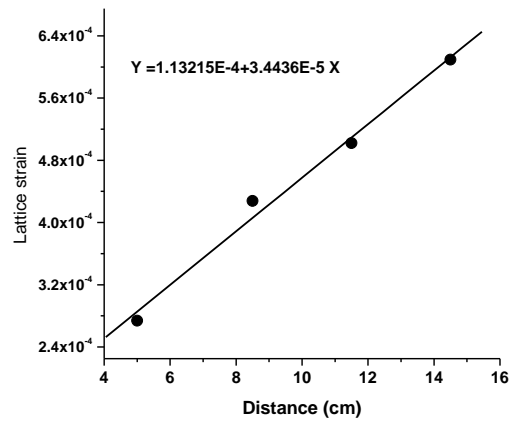


Fig. 9: lattice strain as a function of inter-electrode distance

The optical characterization of the ZnSe thin films of inter-electrode distance has been performed from spectral absorbance (α) in the wavelength range extended from 400 to 1100 nm as shown in Fig. 10. The optical absorption data were analyzed using the following classical relation for near edge optical absorption in a semiconductor,

$$\alpha(h\nu) = \frac{K(h\nu - E_g^{opt})^{n/2}}{h\nu}$$

Where k is a constant, E_g^{opt} is a semiconductor band gap and n a constant equal to 1 for direct transitions and 4 for indirect transition compounds [23]. The variation of $(\alpha \cdot h\nu)^2$ vs. $(h\nu)$ for the sample is shown the Fig. 11. The nature of the graphs reveals that the optical absorption in this sample takes place through direct inter band transitions. The extrapolation of the linear portion of the curve to zero absorption coefficient gives the value of optical band gap energy. The E_g^{opt} increase with increasing inter-electrode distance as shown in Fig. 12. This increasing may be attributed to the increase in both crystallites size and lattice strain. increasing inter-electrode distance of the films are characterized by more homogeneous network, which reduce the number of defects and localized states, and thus the energy gap increases.

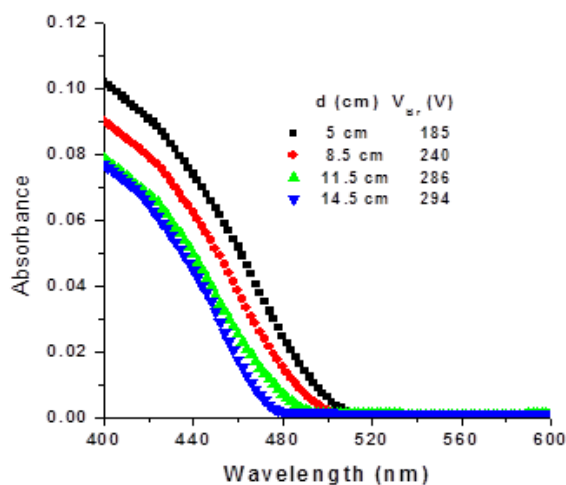


Fig. 10: Absorbance spectra at minimum value Paschen's curves of Ar, at different inter-electrode distances.

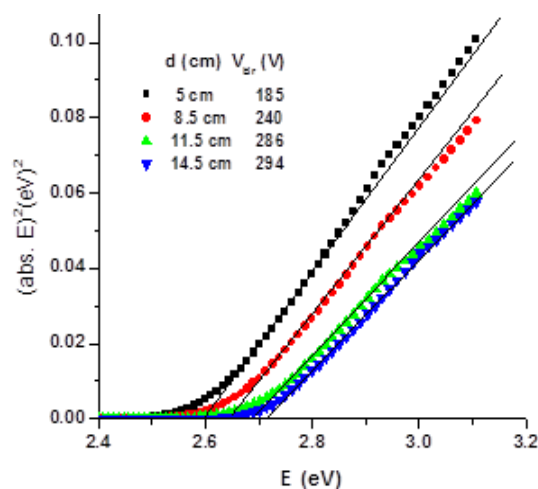


Fig. 11: $(\text{abs. } E)^2$ versus E spectra at minimum value Paschen's curves of Ar, at different inter-electrode distances

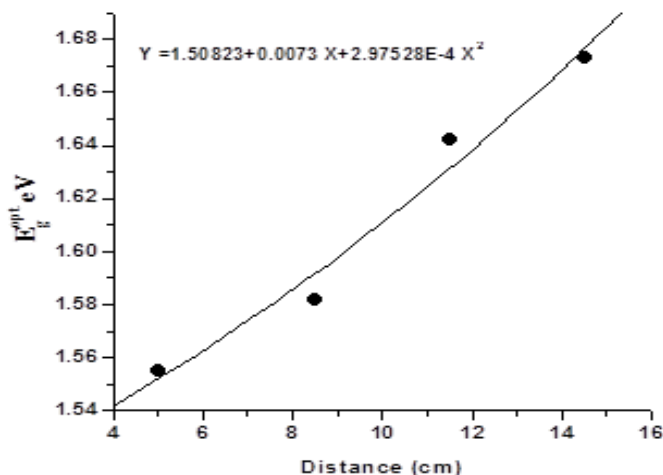


Fig. 12: Optical band gap as a function at minimum value Paschen's curves of Ar, at different inter-electrode distances

4 Conclusions

A glow discharge device is constructed and operated by using Ar gas. Paschen curve is analyzed at different pressures and inter-electrode distances. The minimum breakdown potential for the cathode occurs at the value of pd_{\min} equal to (0.5 torr cm) for Ar discharge. The effect of exposure to the Ar plasma immersion-ion-implantation at different inter-electrode spacing (5, 8.5, 11.5 and 14.5 cm) on the microstructure parameters and energy gap of ZnSe thin film are investigated. Both crystallite size and lattice strain increase with increasing the inter-electrode distance due to the reduction of FWHM. The increasing in crystallite size may attribute to the decreasing in the FWHM at each reflection when the increasing of the inter-electrode distance and also may be interpreted in terms of a columnar grain growth. Furthermore the microstrain displays the same behavior i.e. increasing with increasing the inter-electrode distance. The microstrain behavior may be due to the decrease in lattice defects among the grain boundary. The optical characterization of the ZnSe thin films of inter-electrode distance has been performed from spectral absorbance (αt) in the wavelength range extended from 400 to 1100 nm. The E_g^{opt} increase with increasing inter-electrode distance. This increasing may be attributed to the increase in both crystallites size and lattice strain. increasing inter-electrode distance of the films are characterized by more homogeneous network, which reduce the number of defects and localized states, and thus the energy gap increases.

References

- [1] M. Anandan et al., *IEEE Trans., Electron Devices*, ED-28, 1035–1042 (1981).
- [2] L. Ledernez, UF. Olcaytug, H. Yasuda, G. Urban, 29th ICPIG, July 12-17, Cancun, Mexico (2009)
- [3] F. Ghaleb, A. Belasri, *EPJ Web of Conferences*, ICNP'1 – 1st International Conference On Numerical Physics 44 (2013)
- [4] V. A. Lisovski and S. D. Yakovin, *Technical Physics*, 45(6) 727–731 (2000).
- [5] M. A. Saady, A. I. Eatah and M. M. Masoud, *Fizikaa* 14(3) 225–232 (2005).
- [6] R. Niedrist, R. Schrittwieser, C. Ionita, 40th EPS Conference on Plasma Physics, July 1-5, Espoo, Finland (2013).
- [7] L. F. Berzak, S. E. Dorfman and S. P. Smith, *Paschen's Law in Air and Noble Gases*, April 25, (2006).
- [8] Annemie Bogaerts, Erik Neyts, Renaat Gijbels, Joost van der Mullen, *Spectrochimica Acta Part B* 57, 609–658 (2002).
- [9] Lisovskiy, V.A. and Y. egorenkov, *Appl. Phys.*, D33, (2000).
- [10] Mohammed K. Khalaf, Ibrahim. R. Agool, Shaimaa H. Abd Muslim, *IJAIEEM*, 3(8), 113-119 (2014).
- [11] Speranza, A., et al, *Meccanica*. 46, 681–697 (2011).
- [12] E. D. Nicholson, *Gold Bull.* 12, 161 (1979).
- [13] M. Ohring, “*Materials Science of Thin Films*”, 2nd edition, Academic Press, USA (2002) (ISBN: 0125249756).
- [14] Rod S Mason and Melanie Pichiling, *J. Phys. D. Appl Phys.* 27, 2363-2371 (1994).
- [15] M. Nastasi, J. Mayer, J.K. Hirvonen, "Ion-Solid Interactions: Fundamentals and Applications," Cambridge Solid State Science Series, Cambridge University Press, Cambridge, UK (2004), (ISBN: 9780521616065).
- [16] J. L. Vossen, *J. Phys. E: Sci. Instrum.*, 12, 1979.
- [17] J. J. Zhu, Y. Kolytyn and A. Gedanken, *Chem. Mater.* 12(1) 73-78 (2000).
- [18] S. Zhao, F. Ma Z. Song and K Xu, *Optical Materials* 30(6), 910-915 (2008).
- [19] L. Eckertová, *Physics of Thin Films*, Springer Science & Business Media (2012).
- [20] E. R. Shaaban, I. Kansal, S. H. Mohamed and J. M. F. Ferreira, *Physica B: Condensed matter* 404, 3571 (2009).
- [21] M. El-Hagary, M. Emam-Ismael, E. R. Shaaban and I. Shaltout, *J. Alloy Comp.* 485, 519 (2009).
- [22] E. R. Shaaban, E. A. A. Wahab and M. Ahmed, *Phys. Scr.* 88(1), 015703 (2013).
- [23] J. Townsend, "Electricity in Gases", Oxford University Press, New York, USA (1915).
- [24] G. K. Williamson and H. W. Hall, *Acta Metallurgica*, 1:22 (1953).
- [25] D.G. Morris, M. A. Morris and M. LeBoeuf, *Materials Science and Engineering: A* 156(1), 11-19 (1992).
- [26] G. H. Chen, C. Suryanarayana and F. H. Froes, *Metallurgical and Materials Transactions* 26(6), 1379-1387 (1995).
- [27] E. Szewczak, J. Paszula, A. V. Leonov and H. Matyja, *Materials Science and Engineering A* A226-228, 115-117 (1997).
- [28] E. R. Shaaban, *J. Alloys Compd.* 563, 274-279 (2013).